Effects of Zn and Mn Promotion in Fe-Based Catalysts Used for CO_X Hydrogenation to Long-Chain Hydrocarbons

Leonardo Falbo,[†ID] Michela Martinelli,[†] Carlo Giorgio Visconti,*[,†ID] Luca Lietti,*[,†] Pio Forzatti,[†ID] Claudia Bassano,[‡] and Paolo Deiana[‡]

[†]Laboratory of Catalysis and Catalytic Processes (LCCP), Politecnico di Milano, Department of Energy, Via La Masa 34, 20156 Milano, Italy
[‡]ENEA, Via Anguillarese 301, 00123 S. Maria di Galeria, Roma, Italy

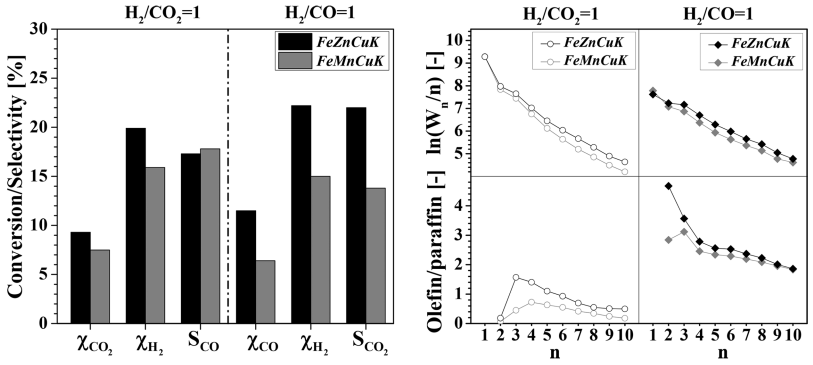

The promoting effect of Mn and Zn on the performance of Fe-based catalysts has been comparatively investigated in the CO_x hydrogenation to heavy hydrocarbons in the presence of H_2-deficient streams. To this scope, two catalysts have been prepared by coprecipitation, followed by impregnation with Cu and K, and tested at 220 °C and 30 bar_g after an activation treatment with syngas. Both catalysts have been found to be active and selective to long-chain hydrocarbons in the presence of either H_2/CO or H_2/CO_2 mixtures. Despite lower catalyst reducibility, the presence of Zn has resulted in higher CO_x conversion rates. Furthermore, the Zn-promoted catalyst converted CO_x into heavier and less-saturated hydrocarbons. These results are consistent with a role of Zn in promoting the catalyst basicity, which is a key property to keep low the superficial H/C ratio and to slow chain termination reactions as well as secondary olefin hydrogenations.

1. INTRODUCTION

Iron-based catalysts are traditionally used in the conversion of synthesis gas (H_2/CO) into chemicals and liquid fuels through the Fischer−Tropsch (FT) synthesis.[1−3] Indeed, although Fe-based catalysts are less active than Co-based catalysts,[4] they are characterized by an intrinsic water−gas shift (WGS) activity. This behavior makes them particularly suitable for the conversion of H_2-deficient syngas like that derived from coal or biomass gasification.[5] More recently, the intrinsic reverse water−gas shift (RWGS) activity of Fe-based catalysts has made these materials of interest also for the one-pot hydrogenation of carbon dioxide into C_{2+} hydrocarbons.[6−9]

Unpromoted bulk iron catalysts present some limits in CO_x hydrogenation stability, activity, and selectivity to hydrocarbon products.[4] In particular, they are characterized by a fast deactivation and a rather high selectivity to light hydrocarbons.[10] Accordingly, alkali metals (K, Na, Cs, Rb), inorganic oxides (Al_2O_3, SiO_2), and transition metals (Cu, Ru, Zn, Mn) are usually included in the catalyst formulation to improve both the resistance to deactivation and the selectivity to long-chain hydrocarbons.[5,11]

Alkali promoters increase surface basicity, strengthening CO and CO_2 adsorption capabilities. This results in higher FT and WGS activities and shifts the selectivity toward olefins and higher molecular weight hydrocarbons.[12,13] Furthermore, alkali metals favor the formation of iron carbides during the catalyst activation process[14,15] (usually carried out with CO or CO/H_2 mixtures[16,17]), which are reported to be the active species in FT synthesis.[18] Among alkaline elements, potassium is reported to be the most effective.[19] Inorganic oxides increase the surface area of the catalyst, avoid the active phase sintering, and improve the attrition resistance.[4,20−22] Eventually, transition metals such as Cu and Ru facilitate the reduction of Fe^{3+} to Fe^{2+} and Fe^0, which are key steps in the formation of iron carbides during the catalyst activation process.[22,23] Furthermore, Cu promotion boosts the WGS activity.[11]

Special Issue: Tapio Salmi Festschrift
Received: April 10, 2017
Revised: June 30, 2017
Accepted: July 3, 2017
Published:July 3, 2017

Among the transition metal promoters of Fe-based catalysts, zinc and manganese are also reported.[24,25] Zinc increases the catalyst surface area[11,26] and forms the $ZnFe_2O_4$ spinel phase, which inhibits sintering during both the catalyst synthesis and activation.[22] Nevertheless, $ZnFe_2O_4$ is catalytically inactive in CO_x hydrogenation processes,[11] and hence, the fraction of iron used to form such compound does not contribute to catalyst activity. In this regard, catalysts with variable Zn/Fe ratios have been considered in the scientific literature to find the value granting stability and the maximum CO_x hydrogenation rate. To date, Zn/Fe molar ratios of about 0.1 are considered optimal for both CO[11] and CO_2[27] hydrogenation processes.

The stabilizing effect of manganese is also explained considering that manganese oxides can form mixed lattices with iron oxides. Manganese is indeed a polyvalent element: as a result, Mn^{3+} ions can be incorporated into the α-Fe_2O_3 lattice as replacement of Fe^{3+} ions, forming a solid solution.[28] Also, Mn^{2+} can be a substitute of Fe^{2+} ions in Fe_3O_4, which results in the formation of a $MnFe_2O_4$ mixed spinel.[29]

The nature of the compounds resulting from the interaction of $Mn^{\delta+}$ and Zn^{2+} with iron is strongly influenced by the adopted preparation method and the oxidation state of metals in the precursor salts.[29,30] In this regard, Soled et al.[22] prefer zinc to manganese because, as a result of its unique oxidation number, zinc maintains its divalent state during controlled pH coprecipitation, thereby facilitating the formation of the ternary oxide. On the contrary, manganese easily oxidizes and induces phase segregation.

A very controversial topic is the electronic effect of Mn and Zn promoters on the nature of Fe-based active species and the catalytic consequences during CO_x hydrogenation. When comparing the performance of unpromoted and Zn-promoted samples, some authors report that Zn increases the catalyst basicity and therefore the olefin selectivity during CO_x hydrogenation.[31] Others report that Zn affects only the CO_x hydrogenation activity, without changing the product selectivity.[11] The same debate is open for the electronic effects of manganese during CO[20,30,32−35] and CO_2[36,37] hydrogenation processes. Some authors propose that small amounts of Mn promote catalyst reduction,[35] catalyst activity,[30] and formation of olefins by increasing the surface basicity.[34] However, these effects are not confirmed by other authors.[38,39]

The comparison of the catalytic performance of Zn- and Mn-promoted Fe-based samples in CO and CO_2 hydrogenation is a topic only partially addressed in the literature.[26−28] With the scope of identifying the most effective promoter, in this work, the effects of Zn or Mn incorporation in the structure of a Fe-based catalyst prepared via coprecipitation are comparatively studied during CO_x hydrogenation at low temperature and high pressure. In particular, the effects of the presence of these promoters are investigated on CO_x conversion and product selectivity under both transient and steady-state conditions.

2. EXPERIMENTAL SECTION

2.1. Catalyst Preparation. Following the procedure reported in ref 40, Fe−Zn and Fe−Mn mixed oxides were prepared by coprecipitation of oxyhydroxides from a mixture of iron(III) and zinc(II) or manganese(II) nitrates, respectively. The incipient wetness impregnation (IWI) technique was used to promote the obtained solids with copper and potassium.

More into details, an aqueous solution of $Fe(NO_3)_3{\cdot}9H_2O$ (Aldrich, ≥ 98%, 3 M) was mixed with an aqueous solution of $Me(NO_3)_2{\cdot}xH_2O$ (Me = Zn or Mn, Aldrich, ≥ 97%, 1.4 M) to obtain a solution containing a Me/Fe atomic ratio of 0.1. The solution was dripped into a jacketed quartz reaction cell kept at 80 °C and containing a buffer solution ($(NH_4)_2CO_3$ 1.0 M, Aldrich, ≥ 30% NH_3 basis) acidified at pH 7 with diluted nitric acid (Aldrich, 65%). A solution of $(NH_4)_2CO_3$ 1.0 M was contemporarily added to the cell through an electronic titrator (Metrohm, Titrino plus) to keep the pH of the slurry at a constant value of 7 ± 0.2. The obtained slurry was filtered, and the obtained solid was washed five times with deionized water (155 cm^3/g_{Fe} each time) at room temperature. The washed sample was dried in static air at 120 °C overnight and calcined in stagnant air at 350 °C for 1 h (heating rate 1 °C/min). The obtained materials ("precursors") were named *FeZn* and *FeMn*.

Copper (Cu/Fe = 0.01 atomic ratio) and potassium (K/Fe = 0.04 atomic ratio) were then added to the precursors by two consecutive IWI steps, using aqueous solutions of $Cu(NO_3)_2{\cdot}3H_2O$ (Aldrich, ≥ 98%) and K_2CO_3 (Aldrich, ≥ 99%) in the first and second impregnation step, respectively. After each impregnation step, the samples were dried in static air at 120 °C overnight, while only after the impregnation with potassium the samples were also calcined in stagnant air at 400 °C for 4 h (heating rate 1 °C/min). The final nominal atomic compositions of the prepared catalysts were 100Fe/10Zn/1Cu/4K and 100Fe/10Mn/1Cu/4K. In the following, these two samples will be referred to as *FeZnCuK* and *FeMnCuK*, respectively.

2.2. Catalyst Characterization. The two catalysts and their precursors were characterized to evaluate their textural, structural, and morphological proprieties. Textural properties were determined by N_2 adsorption−desorption at 77 K. Adsorption and desorption isotherms were measured by using a Micromeritics Tristar 3000 instrument. Prior to these analyses, the samples were treated under vacuum at 120 °C for 3 h.

Powder X-ray diffraction analyses were carried out using a D8-Advance Bruker diffractometer and Cu Kα radiation (λ = 1.54 Å). A scan rate of 0.05° per step and a scan time of 12.5 s^{-1} over a 2θ range of 20−70° were adopted.

The reducibility of the obtained catalysts was measured by temperature-programmed reductions in hydrogen (H_2-TPR), using a Thermo Scientific TPDRO 1100 instrument. Prior to each test, the powdered catalyst was placed in a quartz reactor (i.d. = 9.6 mm) and treated with 20 $L(STP)/h/g_{cat}$ of 20 vol % O_2 in Ar (Sapio), heating from ambient temperature to 400 °C at 10 °C/min and then holding at 400 °C for 1 h. The sample was then cooled to ambient temperature in flowing He. The feed gas was then switched to 20 vol % H_2 in Ar (Sapio, 40 $L(STP)/h/g_{cat}$), and the reactor temperature was increased to 800 °C at 10 °C/min. Hydrogen consumption was monitored by a thermal conductivity detector (TCD), placed downstream of the reactor after a soda lime trap to remove water formed in the reduction process.

2.3. Catalyst Testing. Activity tests were carried out in a lab-scale plant equipped with a fixed-bed reactor, working 24/7. More details on the experimental rig and on the process analytics can be found elsewhere.[9,40] We recall here that gaseous products were periodically analyzed using an online gas chromatograph (Agilent, 7820A) equipped with four columns and two detectors used to quantify H_2, Ar, N_2, CH_4, CO, CO_2, and C_2−C_{10} hydrocarbons. Organic oxygenates, which accounted for less than 10% of consumed CO and CO_2, were neglected.

Table 1. Process Conditions Adopted in CO_x Hydrogenation Tests

	#1	#2	#3
condition	$H_2/CO = 2$	$H_2/CO_2 = 1$	$H_2/CO = 1$
T [°C]	220	220	220
GHSV [$L(STP)h^{-1}g_{cat}^{-1}$]	6	6	6
P [bar_g]	30.0	30.0	30.0
P^0_{H2} [bar_g]	19.2	9.6	9.6
P^0_{CO} [bar_g]	9.6	–	9.6
P^0_{CO2} [bar_g]	–	9.6	–
P^0_{N2} [bar_g]	–	10.8	10.8
P^0_{Ar} [bar_g]	1.2	–	–

In a typical run, 0.5 g of catalyst, diluted with α-Al_2O_3 powders (obtained by calcination at 1400 °C for 8 h of Sasol Puralox SCCa powders) to obtain a catalyst/inert dilution ratio of 1/10 v/v, was activated in situ at 270 °C (heating ramp = 1 °C/min) for 1 h, flowing syngas (H_2/CO = 2 mol_{H2}/mol_{CO}, GHSV = 6 $L(STP)/h/g_{cat}$) at atmospheric pressure. After the activation step, the reactor was cooled to 220 °C, and the pressure was slowly increased to the value of 30 bar_g. These process conditions (condition #1, Table 1) were kept unchanged until conversion and product distribution reached steady-state conditions, i.e., a variation of conversion and selectivity below 1% per day.

The effect of Zn or Mn in the catalyst formulation on the reactivity of H_2-deficient CO_x/H_2 mixtures was then investigated by keeping constant the H_2 partial pressure (9.6 bar_g) and the H_2/CO_x molar ratio in the feed (1 mol_{H2}/mol_{COx}). In particular, activity tests were performed in the presence of $H_2/CO_2/N_2$ (32/32/36 v/v) and $H_2/CO/N_2$ (32/32/36 v/v) mixtures (conditions #2 and #3, Table 1), keeping constant the other process conditions (T = 220 °C, P = 30 bar_g, GHSV = 6 $L(STP)/h/g_{cat}$). During all tests, the approach to WGS equilibrium was considered: the catalysts always worked far from this condition.

Carbon selectivity to the i^{th} (S_i) was calculated according to eq 1, while the value of hydrogen to CO_x usage ratio (U.R.) was calculated according to eq 2

$$S_i = \frac{F_i^{out} n_i}{F_{CO}^{in}\chi_{CO} + F_{CO_2}^{in}\chi_{CO_2}} \quad (1)$$

$$\text{U.R.} = \frac{\chi_{H_2}}{\chi_{CO} + \chi_{CO_2}} \frac{F_{H_2}^{in}}{F_{CO}^{in} + F_{CO_2}^{in}} \quad (2)$$

In eqs 1 and 2 F_i^{out} and n_i are the molar flow and the carbon number of i^{th} species leaving the reactor, respectively. Also, F_{CO}^{in}, $F_{CO_2}^{in}$, and $F_{H_2}^{in}$ are CO, CO_2, and H_2 inlet molar flows, respectively, and χ_{CO}, χ_{CO_2}, and χ_{H_2} are CO, CO_2, and H_2 conversions, respectively.

3. RESULTS AND DISCUSSION

3.1. Catalysts Characterization. XRD patterns (Figure 1) show that both *FeZn* and *FeMn* samples contain amorphous/microcrystalline α-Fe_2O_3 phase (hematite) and mixed spinels: zinc ferrite in one case, manganese ferrite in the other.

The two samples have similar textural properties (Table 2) with BET areas slightly higher than 160 m^2/g, pore volumes around 0.3 cm^3/g, and average pore diameters slightly smaller than 70 Å. Both samples have IV type isotherm with H1 type hysteresis (Figure 2(a)) accordingly to IUPAC classification.

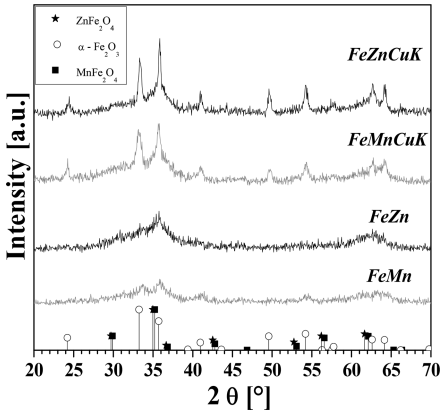

Figure 1. XRD patterns for precursors and catalysts.

Table 2. Textural Properties of Precursors and Catalysts

	surface area [$m^2\ g^{-1}$]	pore volume [$cm^3\ g^{-1}$]	average pore diameter [Å]
FeZn	161	0.26	65
FeMn	164	0.28	68
FeZnCuK	114	0.25	88
FeMnCuK	129	0.26	82

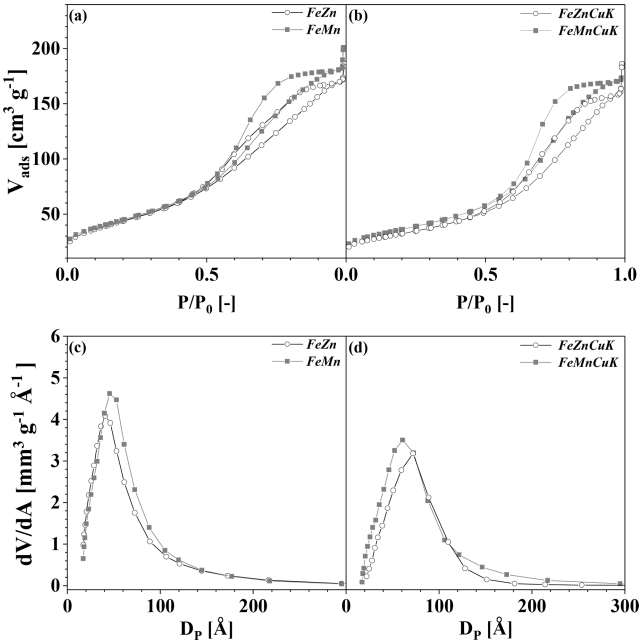

Figure 2. N_2 isotherms (a, b) and pore size distributions (PSDs) for the adsorption branch (c, d).

Pore size distributions (PSDs), derived by using the BJH approach from the adsorption branch (Figure 2(c)), are also very similar for the two precursors, showing unimodal trends centered in the 20−100 Å range.

Figure 1 also shows the XRD spectra of both *FeZnCuK* and *FeMnCuK* catalysts. These samples are more crystalline than the corresponding precursors. In particular, XRD patterns of both the samples show sharp peaks associated with a crystalline α-Fe_2O_3 phase (2θ = 24.4°, 33.2°, 35.7°, 49.6°, 54.2°). As shown in a previous work by some of us,[40] this is due to the calcination at 400 °C carried out on the precursor samples after the impregnation with potassium. Zinc and manganese ferrites, on the contrary, remain microcrystalline. No peaks associated with K- and Cu-containing species are detected, possibly because of their low concentration and good dispersion. The crystallite sizes for the α-Fe_2O_3 phase, calculated with the Scherrer's formula on the peak at 2θ = 49.6° is 24 nm for the *FeZnCuK* sample and 16 nm for the *FeMnCuK* catalyst, respectively. Similar results, with a variation of less than ±2 nm have been obtained considering the peaks at 2θ = 24.4°, 33.2°, and 54.2°.

As result of the higher crystallinity, the catalysts show lower specific surface areas (<130 m^2/g) and bigger average pore sizes (>80 Å) than the corresponding precursors (Table 2). This can also be observed in the N_2 adsorption−desorption isotherms (Figure 2(b)) and PSDs, (Figure 2(d)), which show broader features than in the case of the corresponding precursors.

Figure 3(a) shows the H_2-TPR profiles of the two catalysts. Two separate H_2 consumption peaks are detected with both the

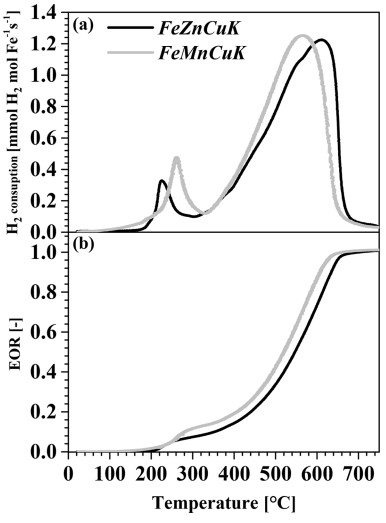

Figure 3. (a) H_2-TPR profiles and (b) EOR profiles for *FeZnCuK* (black line) and *FeMnCuK* (gray line) catalysts.

samples, one centered at temperatures between 200 and 300 °C and the other at temperatures between 400 and 650 °C. In line with literature indications,[11,20,41] the first peak corresponds mostly to the reduction of α-Fe_2O_3 to Fe_3O_4 (partial reduction of Fe^{3+} to Fe^{2+}), while the second peak corresponds to the reduction of Fe_3O_4 (magnetite) to Fe^0 (metallic iron). This latter peak is rather complex because it involves the transformation of a mixture of Fe^{3+} and Fe^{2+} into metallic iron. Moreover, our catalysts also contain $ZnFe_2O_4$ or $MnFe_2O_4$ phases, whose reduction is reported to proceed through a sequence of steps involving at first a phase segregation of Fe_3O_4 and ZnO or MnO and then the Fe_3O_4 reduction.[29,41] Typically, the formation of FeO is not observed because this species is metastable.[42]

The comparison of the H_2-TPR profiles of the two catalysts shows that the promoter nature affects iron reducibility. In particular, the onset of the first peak occurs at 100 °C for the Mn-containing catalyst and at 175 °C for the Zn-containing catalyst. Similarly, the second peak reaches its maximum at 550 °C for the *FeMnCuK* sample and at 610 °C for the *FeZnCuK* catalyst. These differences can be tentatively associated with the different crystallite size of the two catalysts.

Figure 3(b) shows the Extent of Reduction (EOR) for the two catalysts as a function of temperature. This parameter is calculated (eq 3) as ratio between the integral amount of hydrogen consumed during H_2-TPR and the theoretical amount required for the complete reduction of Fe, assuming that initially Fe_2O_3 is the only Fe-containing species.

$$\mathrm{EOR}(T) = \frac{\int_0^t (F_{H_2}^{out} - F_{H_2}^{in})\mathrm{d}t}{\nu_{H_2} n_{Fe_2O_3}} \frac{\Delta T}{\Delta t} \tag{3}$$

In eq 3, $F_{H_2}{}^{out}$ and $F_{H_2}{}^{in}$ are the outlet and inlet H_2 molar flows, respectively; ν_{H_2} is the H_2 stoichiometric coefficient for the complete reduction of Fe_2O_3 to Fe^0 (equal to 3); $n_{Fe_2O_3}$ is the molar amount of Fe_2O_3 used for the analysis; and $\frac{\Delta T}{\Delta t}$ is the slope of the heating ramp. The EOR profiles (Figure 3(b)) point out that both catalysts are fully reduced over 630 °C, while at lower temperature the Mn-containing sample reaches a higher EOR.

3.2. Catalysts Reactivity. *3.2.1. Activation.* The flow rates of unconverted reactants (CO, H_2) and C-containing products (CO_2, CH_4) leaving the reactor during the activation treatment of both catalysts are plotted in Figure 4(a) and (b) as a function of Time of Activation (T.o.A.). As expected at atmospheric pressure, no C_{2+} species are detected in the outlet stream. The carbon (ΔC) and hydrogen (ΔH) mole balances, defined according to eqs 4 and 5, are plotted versus the time of activation in Figure 4(c) and (d).

$$\Delta C = F_{CO}^{in} - F_{CO}^{out} - F_{CO_2}^{out} - F_{CH_4}^{out} \tag{4}$$

$$\Delta H = 2F_{H_2}^{in} - 2F_{H_2}^{out} - 4F_{CH_4}^{out} \tag{5}$$

In eqs 4 and 5, F_{CO}^{in} and $F_{H_2}^{in}$ are CO and H_2 flow rates fed to the reactor, respectively, while F_{CO}^{out}, $F_{CO_2}^{out}$, $F_{CH_4}^{out}$,and $F_{H_2}^{out}$ are CO, CO_2, CH_4, and H_2 flow rates leaving the reactor, respectively. Positive values of ΔC indicate that some carbon remains on the catalyst surface. Accordingly, ΔC values can be used as a first approximation to trace the formation of iron carbides. On the contrary, under the hypothesis that no hydrogen is accumulated on the catalyst surface, positive values of ΔH indicate that H_2O is released from reactions occurring on the catalytic bed. Accordingly, ΔH can be used as tracer of the catalyst reduction.

Figure 4(a) and (b) show that no changes in the catalyst occur until a temperature slightly above 120 °C. At this point, a small consumption of H_2 begins for both catalysts, resulting in positive values of ΔH (Figure 4(c) and (d)). By recalling the results of the H_2-TPR, this consumption, which continues until 200−220 °C, can be attributed to the reduction of hematite to magnetite. This interpretation is also confirmed by a quantitative analysis of the areas of the ΔH peaks, which well

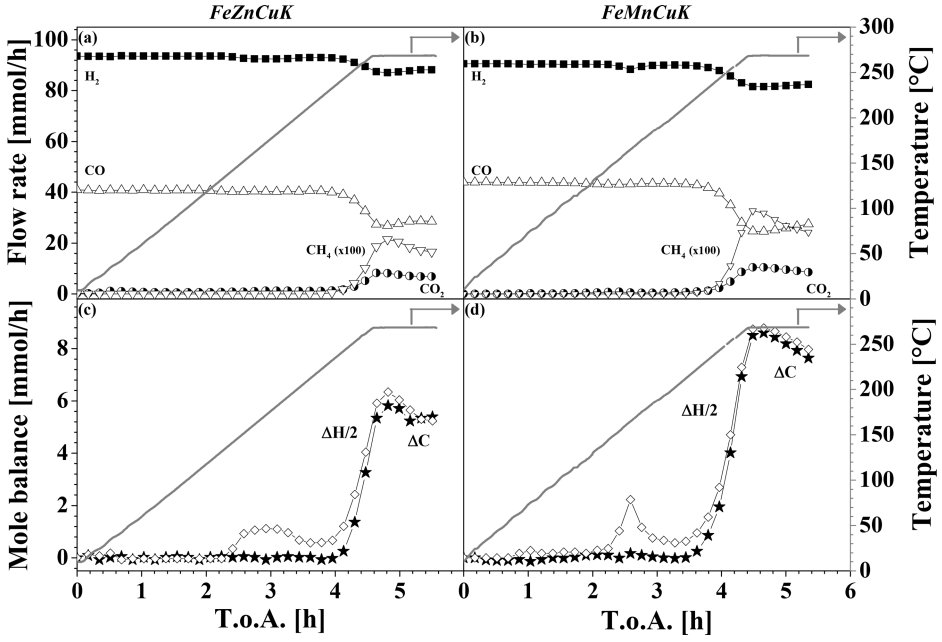

Figure 4. Outlet flow rates during the activation step of (a) *FeZnCuK* and (b) *FeMnCuK*. H and C mole balances for (c) *FeZnCuK* and (d) *FeMnCuK*. Activation procedure: heating from ambient temperature to 270 °C at 1 °C/min and holding at 270 °C for 1 h. P = 0 bar_g, H_2/CO = 2 mol_{H2}/mol_{CO}, GHSV = 6 L(STP)/h/g_{cat}.

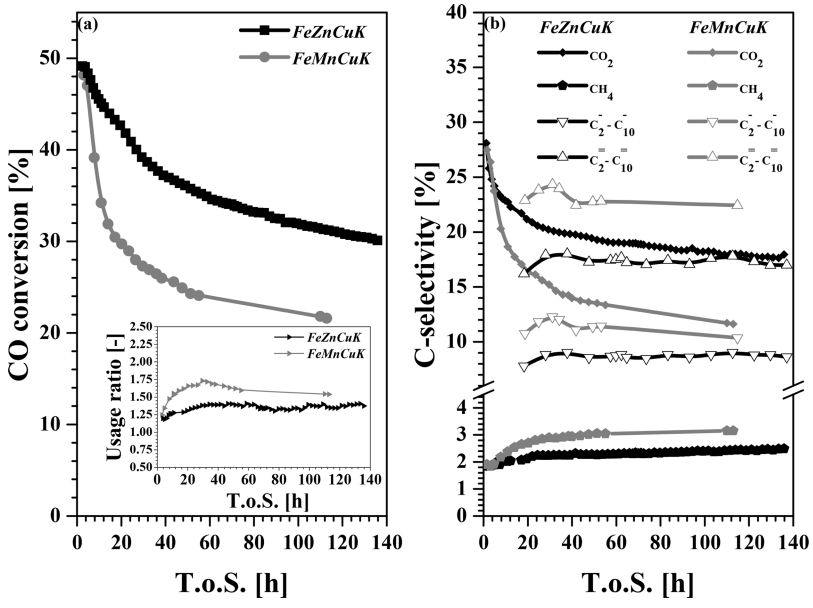

Figure 5. (a) CO conversion, (inset panel (a)) H_2/CO usage ratio and (b) carbon selectivity for *FeZnCuK* and *FeMnCuK* catalysts as a function of T.o.S. (Process condition #1 in Table 1).

correspond to the amounts of H_2 required by the reduction of Fe_2O_3 species to Fe_3O_4.

As observed during H_2-TPR analyses, the onset of this transformation occurs at slightly lower temperature for the Mn-containing catalyst (Figure 4 (a) and (b)).

By increasing the temperature further, phenomena inducing faster CO and H_2 consumptions are observed, and in parallel to these consumptions, CO_2 and CH_4 are formed, with CH_4 molar flow being 2 orders of magnitude lower than that of CO_2. Notably, in parallel to the reduction of magnetite by H_2 (eq 6), the presence of CO_2 in the gas phase may indicate several reactions occurring on the catalyst, including the CO-driven reduction of magnetite to metallic iron (eq 7), the formation of iron carbides (FeC_x, eq 8), and the Boudouard reaction (eq 9).

$$Fe_3O_4 + 4H_2 \rightarrow 3Fe^0 + 4H_2O \quad (6)$$

$$Fe_3O_4 + 4CO \rightarrow 3Fe^0 + 4CO_2 \quad (7)$$

$$Fe^0 + 2xCO \rightarrow FeC_x + xCO_2 \quad (8)$$

$$2CO \rightarrow C + CO_2 \quad (9)$$

Nevertheless, the fact that ΔC is positive in this temperature range (Figure 4(c) and (d)) and that the reduction of magnetite to metallic iron by CO does not cause any variation

in the moles of carbon in the gas phase (1 mol of CO_2 is formed per mole of CO reacted, eq 7) is a clear indication that reactions involving C deposition on the catalyst are occurring (e.g., eqs 8 and 9), possibly in parallel to the magnetite reduction reactions (eqs 6 and 7). The possibility to have a partial hydrogenation of superficial carbon species on carbides has been neglected.

This behavior is in line with the Fischer−Tropsch literature, according to which both iron carburization[43] and the Boudouard reaction[44] occur on reduced iron centers. In this regard, the presence of methane in the stream leaving the reactor during the activation procedure suggests that at least some of the iron centers are transformed into carbides. Indeed, while reduced iron centers as well as iron oxides and Fe−Mn and Fe−Zn mixed spinels are known to be inactive in the synthesis of hydrocarbons,[45] iron carbides are known as the active sites in CO hydrogenation.[18,46]

In line with the higher reducibility of the *FeMnCuK* catalyst with respect to the *FeZnCuK* sample pointed out by H_2-TPR experiments, the onset of Fe_3O_4 reduction occurs at 230 °C for the *FeZnCuK* sample and at a lower temperature (215 °C) for the *FeMnCuK* catalyst. Notably, after their onset, reactions reported in eqs 6−9) continue for the entire T-ramp and also during the isothermal period at 270 °C.

At the end of the activation procedure, the integral amount of carbon deposited on the catalyst surface (either as carbon residue or as iron carbide) for the *FeMnCuK* sample is about 70% higher than that deposited on the *FeZnCuK* sample. At the same time, the CH_4 flow rate from the *FeMnCuK* sample is more than 50% higher than that from the *FeZnCuK* sample: these results suggest that *FeMnCuK* is better carbided than *FeZnCuK*.

3.2.2. Start Up. The CO conversion trends in the first 120 h on stream at 220 °C, 30 bar_g, and $H_2/CO = 2$ mol_{H2}/mol_{CO} (condition #1 in Table 1) are shown in Figure 5(a) for both Mn- and Zn-containing catalysts. The selectivity of the two catalysts in the same period of time is shown in Figure 5(b).

Notably, in the early hours on stream, regardless the different quantitative behavior during the activation treatment, the two catalysts are characterized by similar CO conversion values (around 50%). The carbon selectivity of the two catalysts is also rather similar, with CO_2 accounting for 28% of the carbon in the products, CH_4 around 2%, and the rest being mostly unsaturated C_{2+} hydrocarbons. As a matter of fact, the H_2/CO usage ratio (U.R., inset of Figure 5(a)) for the two catalysts is about 1.3. Such a value is lower than expected considering the FT stoichiometry (eq 10) and can be explained taking into account the stoichiometry WGS reaction (eq 11), which forms H_2 and consumes CO.

$$CO + 2H_2 \rightarrow \frac{1}{n}(-CH_2 -)_n + H_2O \quad (10)$$

$$CO + H_2O \leftrightarrow CO_2 + H_2 \quad (11)$$

This result suggests that the carbidization degree at the end of the activation treatment is not necessarily representative of the catalyst activity at higher pressure and lower temperature. We speculate that surface reconstruction and/or catalyst carbidization/decarbidization during the reactor pressurization and cooling may be responsible for this behavior.

In the first 120 h on stream, both catalysts progressively lose activity. At the same time, the process selectivity changes, with the CO_2 content significantly decreasing and the selectivity to C_1-C_{10} hydrocarbons as well as the usage ratio increasing. Notably, the faster deactivation, accompanied by the most important change in performance, is observed in the case of the Mn-promoted sample, which loses 50% of its initial activity in 120 h (vs 35% in the case of the Zn-promoted sample) and whose U.R. grows to 1.5.

The evolutions of catalyst activity and selectivity with Time on Stream (T.o.S.) suggest that deactivation phenomena occur for both catalysts during the start up. These phenomena are well known for the Fe-based FT catalysts[10] and usually attributed to four deactivation causes:[47−49] (i) deposition of carbonaceous materials ("fouling"), (ii) transformation of catalytically active species into less active or inactive forms ("reconstruction"), (iii) loss of surface area due to crystallite growth ("sintering"), and (iv) poisoning of the surface by sulfur compounds, heavy metals, or chlorines.

Mechanism (iv) can be ruled-out in our case due to the high purity of the syngas fed to the reactor. Also mechanism (iii) is expected to be minor on our catalysts considering that Zn and Mn are added to Fe-based catalysts to protect them from sintering.[22,24,25] On the contrary, our data seem in line with the presence of deactivation mechanisms (i) and (ii). Mechanism (i) seems to dominate the deactivation in the first 30 h on stream. In this period of time, as a consequence of the progressive carbon deposition through the Boudouard reaction (eq 9), CO conversion decreases (Figure 5(a)), as well as hydrocarbon yields (data not shown). CO_2 selectivity is very high (Figure 5(b)), being this species responsible for the O rejection from the catalytic surface. Note that, in this period of time, carbon balance (defined as the ratio among the carbon in the products and the converted carbon) closes below 1, as a consequence of the "loss" of some carbon, which remains on the catalyst bed. The deactivation rate decreases with T.o.S. as a consequence of the progressive slowing of carbon deposition reactions, whose active sites are progressively poisoned by deposited carbon. As a result of the major loss of sites active in the Boudouard reaction, hydrocarbon selectivities progressively grow, while CO_2 selectivity quickly decreases (Figure 5(b)).

The Mn-promoted sample is affected more than the Zn-containing catalyst by this initial deactivation, possibly as a result of the presence on its surface of a major amount of reduced (but uncarbided) Fe sites[10] which promote the Boudouard reaction.[44]

After the first 30 h on stream, the reactivity of our catalysts suggests that the Boudouard reaction occurring on Fe^0/Fe_3O_4 sites becomes progressively slower. Indeed, in this period of time, CO_2 selectivity is much lower than in the first 30 h on stream, and the activity loss is accompanied only by minor variations of both process selectivity and usage ratio. However, an unselective deactivation mechanism still remains active, which brings the loss of some catalytic sites without affecting the activity and selectivity of the remaining sites[40] (mechanism (ii)).

Notably, the deactivation rate (loss of CO conversion with time) in the 30−120 h time interval is very similar for the two catalysts we tested. However, as a consequence of the lower WGS activity (we return to this point later), in this period of time, the Mn-promoted sample is more selective to hydrocarbons than the Zn-containing catalyst.

At 120−140 h on stream, both catalysts reached a pseudo-steady-state condition. Indeed, in this period of time, the CO conversion decreases less than 1% per day for both the samples. Reactants conversion and CO_2 selectivity are reported in Table

3 (condition #1). After this period of time, the reactor feed was switched to H_2-deficient CO_x-containing streams. During all the tests with H_2-deficient feed streams, the catalysts were very stable, and no deactivation was measured for the whole duration of the tests (~200 h).

Table 3. Steady State Conversion and Selectivity Values Measured during CO_x Hydrogenation Tests[a]

	FeZnCuK			*FeMnCuK*		
condition	#1	#2	#3	#1	#2	#3
species						
			conversion [%]			
CO	31.5	–	11.5	21.8	–	6.4
CO_2	–	9.3	–	–	7.5	–
H_2	22.4	19.9	22.2	14.5	15.9	15.0
			selectivity [%]			
CO	–	17.3	–	–	17.8	–
CO_2	17.8	–	22.0	11.6	–	13.8

[a]Process conditions given in Table 1.

3.2.3. Reactivity with $H_2/CO_2/N_2$ Mixture. To verify the catalyst stability in the presence of CO_2, the feed stream was switched at first to H_2/CO_2 = 1 mol_{H2}/mol_{CO2} (condition #2, Table 1) and kept unvaried for 80 h. Both catalysts were found to be stable under these conditions (no deactivation observed in 80 h on stream), even though the hydrocarbon formation rate, as well as the reactant conversions, dropped with respect to those measured in the presence of CO (Table 3).

As in the presence of CO, the Zn-promoted catalyst was found to be more active than the Mn-containing sample. As a matter of fact, by using the *FeZnCuK* catalyst, we measured a CO_2 conversion of 9.3%, while the *FeMnCuK* sample resulted in a CO_2 conversion of 7.5%. These results fully agree with those obtained by Nam et al.,[27,50] who reported a similar relative increase in the catalyst activity (+15%) when replacing Mn with Zn in K-free and Cu-free catalysts. We believe that the motivation of the different reactivity of the two catalysts is the different surface basicity of the two samples, which in turn depends on the electronic effects of Mn and Zn. In particular, we believe that the presence of Zn increases the basicity of the catalyst surface,[27] thus enhancing the CO_2 chemisorption and weakening the H_2 chemisorption.[51] This makes the CO_2 conversion rate faster, being that the CO_2 conversion kinetics are usually limited by the small amount of chemisorbed CO_2.[27,52]

Starting from CO_2 and H_2 conversion values, a U.R. of about 2.2 was calculated for the *FeZnCuK* catalyst, while a value of 2.1 was found for the *FeMnCuK* sample. Both these values are lower than that required by the stoichiometry of the CO_2 hydrogenation to hydrocarbons (eq 12).

$$CO_2 + 3H_2 \rightarrow \frac{1}{n}(-CH_2-)_n + 2H_2O \quad (12)$$

Considering that CO_2 is hydrogenated to hydrocarbons via a two-step pathway where CO is the reaction intermediate,[51] observed U.R. values suggest that not all the CO produced by RWGS is hydrogenated to hydrocarbons by FT synthesis. This matches with what has been observed experimentally: CO selectivities of 17.3% and 17.8% were measured in the case of *FeZnCuK* and *FeMnCuK* catalysts, respectively (Table 3).

Notably, considering that both RWGS and FT are far from the thermodynamic equilibrium at the adopted process conditions, similar CO selectivities and U.R. imply similar ratios between RWGS and FT activities for the two tested catalysts. Nevertheless, some differences between the two catalysts exist in terms of hydrocarbon product distribution (Figure 6(a)). In particular, although both catalysts form products following the Anderson–Schultz–Flory (ASF) plot, the slope of the *FeZnCuK* sample is smaller than that of the *FeMnCuK* catalyst, thus indicating a product distribution more shifted toward long-chain products. As a matter of fact, the chain growth probability (α) for the C_3–C_{10} species is 0.65 for

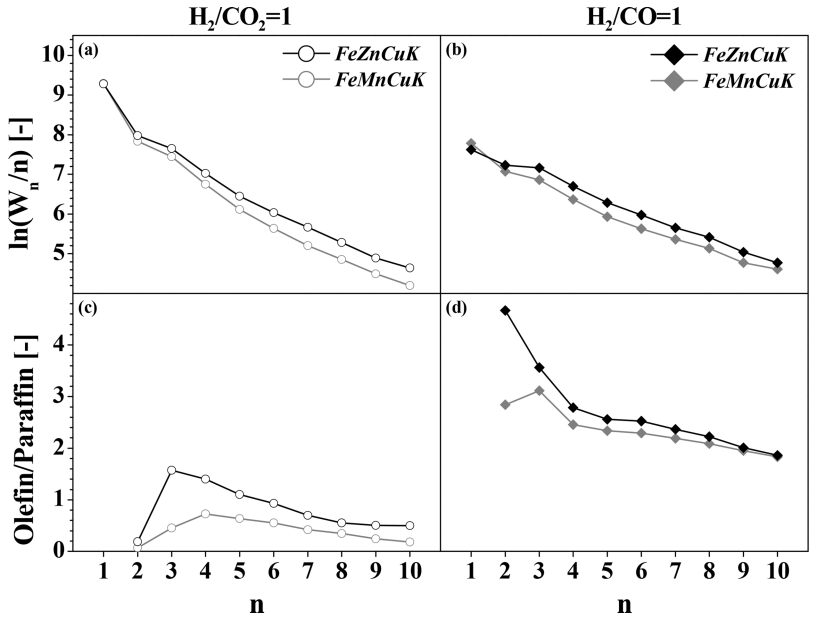

Figure 6. (a) ASF plots (shown in terms of productivity) and (c) olefin/paraffin ratios as a function of the carbon number during CO_2 hydrogenation. (b) ASF plots and (d) olefin/paraffin ratios as a function of the carbon number during CO hydrogenation. (Process conditions #2 and #3 in Table 1).

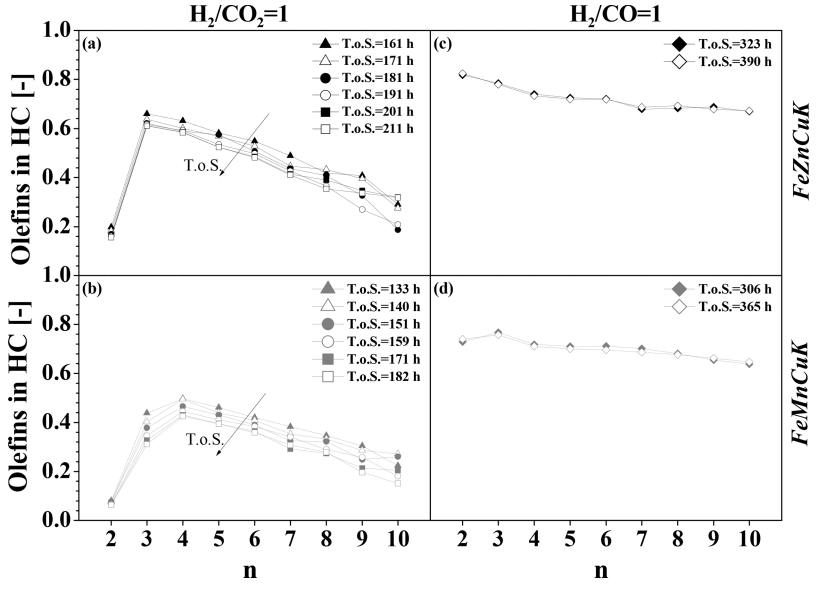

Figure 7. Fraction of olefins in hydrocarbon products as a function of the carbon number during CO_2 hydrogenation ((a) *FeZnCuK* and (c) *FeMnCuK*) and CO hydrogenation ((b) *FeZnCuK* and (d) *FeMnCuK*): evolution with T.o.S. (Process conditions #2 and #3 of Table 1).

the Zn-containing catalyst and 0.61 for the catalyst containing Mn.

Again, the higher selectivity to heavy hydrocarbons of the Zn-promoted sample can be explained considering its higher surface basicity, which enhances CO_2 chemisorption. Indeed, this results in a lower H/C ratio, which is known to be a key parameter in determining the relative ratio of the chain growth reaction rate and the termination reaction rate.

Another relevant difference between the two catalysts is observed in terms of product olefinicity (expressed as olefin to paraffin ratio in the product), shown in Figure 6(b) as a function of the carbon number. First of all, the O/P ratio for *FeMnCuK* is much lower than that of *FeZnCuK* and indicates that the most abundant C_2−C_{10} hydrocarbon products are saturated when using Mn. This is not the case with the Zn-containing sample, where olefins are more abundant than paraffins in the C_3−C_6 range. Again, this underlines the role of Zn in enhancing CO_2 chemisorption, thus limiting the H_2 available on the surface for the formation of saturated hydrocarbons.[12,51]

Also, the O/P distribution is different for the two adopted catalysts. In the case of the *FeZnCuK* catalyst, the O/P ratio monotonically decreases with the carbon number, with the only exception being the C_2 species, which is very low and out of trend. As a result, C_3 is the species with the higher O/P ratio. This is not the case with the Mn-promoted sample, where the maximum in the O/P distribution shifts on C_4.

Notably, the O/P distribution obtained with the Zn-promoted sample during CO_2 hydrogenation looks very similar to those typical of unpromoted Fe-based catalysts under FT conditions,[23] where CO is the most abundant species on the catalyst surface and H_2 adsorption is limited. Such a distribution, which further confirms that the presence of Zn helps in keeping the H/C ratio on the surface low even in the presence of CO_2, is usually explained considering that olefins undergo secondary reactions (hydrogenation to the corresponding paraffins and reinsertion in chain growth mechanism) with a reactivity which increases with the carbon number because of the higher solubility of heavy olefins in the liquid waxes filling the catalyst pores.[53−55] C_2 species are out of trend because of the high reactivity of ethylene.[7,56,57] On the contrary, the O/P distribution obtained with the Mn-containing catalyst is unusual for Fe-based FT catalysts and resembles that observed in our previous works on CO_2 hydrogenation, when catalysts promoted with low amounts of potassium were used.[8,40] In that case, the anomalous O/P trend was explained considered that, in the presence of low amounts of K, metallic iron or oxidized Fe centers remain after the activation treatment and the start up, which are active for the double-bond-shift reactions.[46] These reactions preserve C_4 and longer-chain olefins from secondary reactions, because internal olefins are more difficult to hydrogenate than terminal olefins. However, they are not effective in preserving ethylene and propylene, which do not have internal isomers. Accordingly, the content of C_2 and C_3 olefins in the products is decreased. We believe that a similar mechanism is responsible for the O/P distribution in the case of the Mn-promoted sample. The Mn-containing sample, which contains a higher amount of metallic iron centers with respect to the Zn-promoted sample, preserves butylenes and longer-chain olefins through a double-bond shift but not C_2 and C_3 olefins. This hypothesis is well supported by the analysis of isomers distribution in C_4 olefins: internal isomers account for about 50% of the olefins in the case of the *FeMnCuK* sample, while their concentration is as low as 25% in the products obtained with the *FeZnCuK* catalyst.

To gain more insight on the stability of the adopted catalysts in the presence of H_2-deficient H_2/CO_2 mixtures, Figure 7(a)−(c) show the evolution with T.o.S. of the olefins content in the products in the 80 h of tests in the presence of CO_2/H_2 mixtures. Notably, opposite to CO_2 conversion and ASF product distribution, both of which remain unvaried with T.o.S. (data not shown), the two catalysts form products having an olefinicity slowly decreasing with time on stream. This suggests that the active sites are progressively modified in the presence of CO_2. In particular, considering that α-olefins are formed via a β-H abstraction on the growing alkyl intermediate over iron carbides and can undergo secondary hydrogenation reactions over metallic or oxidized Fe centers,[46] data shown in Figure 7(a)−(c) suggest that some additional sites active in the secondary hydrogenation of olefins are formed during CO_2

hydrogenation. This phenomenon, which is possibly accelerated in the presence of H_2-deficient feed, results in the consequent decrease in olefins in the products.

Our data do not point out strong effects of the adopted promoter in affecting the catalyst evolution with T.o.S., even though the Zn-promoted catalyst seems slightly more resilient, even in consideration of its higher activity. This aspect merits further investigation especially when unsaturated hydrocarbons are the products of interest during CO_2 hydrogenation.[9]

3.2.4. Reactivity with H_2/CO/N_2 Mixture. Following the tests with CO_2, the reactivity of the two catalysts in the presence of a H_2/CO mixture with a unitary molar ratio (condition #3 in Table 1) was investigated for 80 h for comparison purposes.

The two catalysts are stable in the presence of H_2-deficient syngas, and *FeZnCuK* remains the most active (Table 3). At 220 °C and 30 bar_g, it grants a CO conversion of 11.5%, while the *FeMnCuK* catalyst brings CO conversions as low as 6.4%. The higher CO conversion of *FeZnCuK*, which confirms what was already observed during the start-up period in the presence of $H_2/CO = 2$ mol_{H2}/mol_{CO}, results in a higher productivity of C_{2+} hydrocarbons (Figure 6(b)), most of which are olefins (Figure 6(c)).

For what concerns the product distribution, the two catalysts grant similar chain growth probabilities ($\alpha_{C3+} = 0.71-0.72$), but the olefin content in the products obtained with the Zn-containing catalyst is higher (Figure 6(c)). Also, the O/P distribution is different for the two catalysts for what concerns C_2 and C_3 species (Figure 6(d)): the *FeZnCuK* catalyst shows a monotonically decreasing trend, while the *FeMnCuK* catalyst shows a trend going through a maximum in correspondence of the C_3 species.

The behavior of the Zn-promoted sample, which is in line with data shown by Iglesia's and Davis's groups[58,59] for catalysts similar to that investigated in this study, suggests that the secondary reactions of olefins are minor in the presence of H_2-deficient streams. In turn, this suggests that the H coverage of the surface is rather low on Zn-promoted samples at the adopted process conditions.

This is not exactly the case of the Mn-containing catalysts. In line with the results reported in the literature[32,60] for Mn-promoted and unpromoted Fe-catalysts, indeed, C_2 species are slightly out of the O/P trend, meaning that ethylene, the most reactive olefin, still undergoes some secondary reactions, possibly catalyzed by the residual uncarbided Fe sites.

Notably, opposite to what we observed during the start-up period, both catalysts are very stable in the presence of syngas. This is confirmed by Figure 7(c) and (d), showing that the olefin content in the product pool remains stable for the whole duration of the test. This further confirms the literature indications according to which both Zn and Mn are highly effective in slowing the catalyst deactivation in the presence of CO.

Before concluding, it is very interesting to compare the reactivity of Zn- and Mn-promoted catalysts in the presence of carbon-rich CO/H_2 and CO_2/H_2 streams with the same C/H inlet ratio.

In the case of the *FeZnCuK* catalyst, CO conversion is higher than CO_2 conversion (Table 3). However, as evident by comparing the corresponding ASF plots in Figure 6(a) and (b), this does not imply an increased hydrocarbon synthesis activity of the *FeZnCuK* catalyst. On this catalyst, the consumption of CO is faster than that of CO_2 because the WGS rate during CO hydrogenation is faster than the RWGS rate during CO_2 hydrogenation. As a matter of fact, the selectivity to CO_2 is equal to 22.0% during CO hydrogenation, while the selectivity to CO was as low as 17.3% during CO_2 hydrogenation. This is not the case of for the *FeMnCuK* catalyst, which shows a CO_2 selectivity of 13.8% during CO hydrogenation and a CO selectivity of 17.8% during CO_2 hydrogenation.

Notably, the reason why the kinetics of FT on the Zn-promoted catalyst is slower than the kinetics of CO_2 hydrogenation is due again to the very strong CO adsorption. It is known, indeed, that opposite to CO_2 hydrogenation, which has positive order with respect to CO_2,[52] CO hydrogenation has negative order in CO.[61] Accordingly, the higher the CO concentration on the surface is, the lower its conversion rate is. In the presence of CO_2, the CO concentration on the surface remains small and the CO conversion rate is faster.

For what concerns the hydrocarbon product distribution, the two catalysts are more selective to heavy products in the presence of CO than in the presence of CO_2. At the same time, CO-containing streams form more unsaturated products, where olefins constitute at least 75% of the hydrocarbon pool.

As also discussed in a previous work,[8] these results are mostly due to the different adsorption strengths of CO_2 and CO on iron-based catalysts, which form different H/C ratios on the catalyst surface. CO is more strongly bonded to Fe sites than CO_2, and this boosts the chain growth process and preserves the primary olefins. At the same time, however, the lower H coverage during CO hydrogenation makes the FT slower. This phenomenon, which is enhanced when using H_2-deficient feed, results in a decreased hydrocarbon yield and on the contrary favors the WGS rate.

4. CONCLUSION

A direct comparison between Zn- and Mn-containing bulk Fe-based Fischer–Tropsch catalysts was carried out in this work in order to gain insights on the role of these structural and electronic promoters in the CO_x hydrogenation to hydrocarbons, in particular when using H_2-deficient feed streams. This is particularly relevant in view of the development of novel process technologies such as CCU (carbon capture and utilization), PTG (power-to-gas), BTL (biomass-to-liquid) or GTL (gas to liquid) exploiting CO_2-rich natural gas fields, all of which requires to limit the H_2 input to the system. To the scope, two catalysts were prepared by constant pH coprecipitation method, and successively impregnated with Cu and K.

We found that the two catalysts have similar textural and morphological properties, with high surface areas, a prevalence of the crystalline Fe_2O_3 phase, and the presence of $ZnFe_2O_4$ and $MnFe_2O_4$. Nevertheless, the average size of hematite crystallites in Mn-promoted sample is smaller than in Zn-promoted sample. Both catalysts are reducible in H_2, but the presence of Mn promotes the reduction of iron oxides at lower temperatures. We observed that, as a result of the higher reducibility, during the activation (carburization) treatment, more carbon is deposited on the surface, possibly as active carbides, in the Mn-promoted samples.

At 220 °C and 30 bar_g, Zn- and Mn-promoted catalysts show initially (i.e., at low T.o.S.) a similar reactivity. The stability of the two catalysts is however rather different, with the Mn-containing sample which deactivates faster than the Zn-promoted sample. Such a phenomenon has been explained considering that the two "fresh" catalysts promote carbon deposition through a Boudouard-like mechanism, and lose

some of the active sites. The former phenomenon is faster on Mn-promoted sample because of the higher number of reduced and uncarbided Fe^0 sites. Also, less iron oxide species and more Fe^0 species are present in Mn-promoted samples at the end of the activation process.

After a stabilization period of about 80 h, however, both catalysts reach stable performance. Tests in the presence of H_2-deficient CO and CO_2 pointed out that both the catalyst can be successfully employed to make long-chain hydrocarbons and in particular olefins.

We have shown that, due to an increased surface basicity, the presence of Zn in the catalyst formulation improves CO and CO_2 adsorption with respect to Mn. This is a key-aspect also when H_2-deficient feed are used. In the case of CO_2 hydrogenation, this boosts the hydrocarbon yield, possibly favoring the RWGS rate. This is not the case of CO, where the increased CO adsorption kinetically inhibits the FT synthesis and favors the WGS. As a result, Zn-promoted catalyst remains more active than Mn-promoted sample, but the synthesis of hydrocarbons becomes slower than during CO_2 hydrogenation. This penalizes the atomic efficiency of the process if hydrocarbons are the product of interest.

Mn- and Zn-promoted catalysts also differ for their activity in the secondary hydrogenation of olefins. These reactions are quite active in the presence of Mn, possibly as a result of the higher H/C ratio on the catalyst surface due to the weaker CO_x adsorptions. This is not the case of Zn-promoted sample, where the stronger CO_x adsorptions keep the H/C ratio on the surface low. As a result the products are more shifted toward long-chain and unsaturated hydrocarbons in the case of the catalyst promoted with Zn, especially in the presence of CO_2.

Accordingly, our data suggest that, either in CO or CO_2 hydrogenation processes, zinc is preferable to manganese because plays a determinant role in stabilizing the catalyst, thus limiting its initial deactivation, and granting better yields to hydrocarbons.

AUTHOR INFORMATION

Corresponding Authors

*Tel. +390223993297. Fax +390223998566. E-mail: carlo.visconti@polimi.it (C.G. Visconti).

*Tel +390223993272. Fax +390223998566. E-mail: luca.lietti@polimi.it (L. Lietti).

ORCID

Leonardo Falbo: 0000-0002-7140-5756

Carlo Giorgio Visconti: 0000-0001-5205-982X

Pio Forzatti: 0000-0003-1533-7848

Notes

The authors declare no competing financial interest.

DEDICATION

This paper is dedicated to Professor Tapio Salmi in recognition of his outstanding research and academic career, as well as to his fundamental contributions to catalysis and chemical reaction engineering.

REFERENCES

(1) Anderson, R. B. *The Fischer–Tropsch Synthesis*; Academic Press: Orlando, 1984.

(2) Dictor, R. A.; Bell, A. T. Fischer–Tropsch Synthesis over Reduced and Unreduced Iron Oxide Catalysts. *J. Catal.* **1986**, *97*, 121.

(3) Kölbel, H.; Ralek, M. The Fischer–Tropsch Synthesis in the Liquid Phase. *Catal. Rev.: Sci. Eng.* **1980**, *21*, 225.

(4) Dry, M. E. The Fischer–Tropsch Process: 1950–2000. *Catal. Today* **2002**, *71*, 227.

(5) Dry, M. E. Fischer–Tropsch Synthesis over Iron Catalysts. *Catal. Lett.* **1991**, *7*, 241.

(6) Aresta, M.; Dibenedetto, A.; Angelini, A. Catalysis for the Valorization of Exhaust Carbon: From CO_2 to Chemicals, Materials, and Fuels. Technological Use of CO_2. *Chem. Rev.* **2014**, *114*, 1709.

(7) Riedel, T.; Claeys, M.; Schulz, H.; Schaub, G.; Nam, S.-S.; Jun, K.-W.; Choi, M.-J.; Kishan, G.; Lee, K.-W. Comparative Study of Fischer–Tropsch Synthesis with H_2/CO and H_2/CO_2 Syngas Using Fe- and Co-Based Catalysts. *Appl. Catal., A* **1999**, *186*, 201.

(8) Visconti, C. G.; Martinelli, M.; Falbo, L.; Fratalocchi, L.; Lietti, L. CO_2 Hydrogenation to Hydrocarbons over Co and Fe-Based Fischer–Tropsch Catalysts. *Catal. Today* **2016**, *277*, 161.

(9) Visconti, C. G.; Martinelli, M.; Falbo, L.; Infantes-Molina, A.; Lietti, L.; Forzatti, P.; Iaquaniello, G.; Palo, E.; Picutti, B.; Brignoli, F. CO_2 Hydrogenation to Lower Olefins on a High Surface Area K-Promoted Bulk Fe-Catalyst. *Appl. Catal., B* **2017**, *200*, 530.

(10) Eliason, S. A.; Bartholomew, C. H. Reaction and Deactivation Kinetics for Fischer–Tropsch Synthesis on Unpromoted and Potassium-Promoted Iron Catalysts. *Appl. Catal., A* **1999**, *186*, 229.

(11) Li, S.; Li, A.; Krishnamoorthy, S.; Iglesia, E. Effects of Zn, Cu, and K Promoters on the Structure and on the Reduction, Carburization, and Catalytic Behavior of Iron-Based Fischer–Tropsch Synthesis Catalysts. *Catal. Lett.* **2001**, *77*, 197.

(12) Dry, M. E.; Shingles, T.; Boshoff, L. J.; Oosthuizen, G. J. Heats of Chemisorption on Promoted Iron Surfaces and the Role of Alkali in Fischer–Tropsch Synthesis. *J. Catal.* **1969**, *15*, 190.

(13) Anderson, R. B.; Seligman, B.; Shultz, J. F.; Kelly, R.; Elliott, M. A. Fischer–Tropsch Synthesis Some Important Variables of the Synthesis on Iron Catalysts. *Ind. Eng. Chem.* **1952**, *44*, 391.

(14) Arakawa, H.; Bell, A. T. Effects of Potassium Promotion on the Activity and Selectivity of Iron Fischer–Tropsch Catalysts. *Ind. Eng. Chem. Process Des. Dev.* **1983**, *22*, 97.

(15) Dry, M. E.; Oosthuizen, G. J. The Correlation between Catalyst Surface Basicity and Hydrocarbon Selectivity in the Fischer–Tropsch Synthesis. *J. Catal.* **1968**, *11*, 18.

(16) O'Brien, R. J.; Xu, L.; Spicer, R. L.; Davis, B. H. Activation Study of Precipitated Iron Fischer–Tropsch. *Energy Fuels* **1996**, *10*, 921.

(17) Bukur, D. B.; Lang, X.; Rossin, J. A.; Zimmerman, W. H.; Rosynek, M. P.; Yeh, E. B.; Li, C. Activation Studies with a Promoted Precipitated Iron Fischer–Tropsch Catalyst. *Ind. Eng. Chem. Res.* **1989**, *28*, 1130.

(18) Shultz, J. F.; Hall, W. K.; Seligman, B.; Anderson, R. B. Studies of the Fischer–Tropsch Synthesis. XIV. Hagg Carbide as Catalysts. *J. Am. Chem. Soc.* **1955**, *77*, 213.

(19) Ngantsoue-Hoc, W.; Zhang, Y.; O'Brien, R. J.; Luo, M.; Davis, B. H. Fischer–Tropsch Synthesis: Activity and Selectivity for Group I Alkali Promoted Iron-Based Catalysts. *Appl. Catal., A* **2002**, *236*, 77.

(20) Lohitharn, N.; Goodwin, J. G. Effect of K Promotion of Fe and FeMn Fischer–Tropsch Synthesis Catalysts: Analysis at the Site Level Using SSITKA. *J. Catal.* **2008**, *260*, 7.

(21) Dry, M. E.; Ferreira, L. C. The Distribution of Promoters in Magnetite Catalysts. *J. Catal.* **1967**, *7*, 352.

(22) Soled, S. L.; Iglesia, E.; Miseo, S.; Derites, B. A.; Fiato, R. A. Selective Synthesis α-Olefins on Fe-Zn Fischer–Tropsch Catalysts. *Top. Catal.* **1995**, *2*, 193.

(23) Bukur, D. B.; Mukesh, D.; Patel, S. A. Promoter Effects on Precipitated Iron Catalysts for Fischer–Tropsch Synthesis. *Ind. Eng. Chem. Res.* **1990**, *29*, 194.

(24) Fiato, R. A.; Soled, S. L. Fischer–Tropsch Hydrocarbon Synthesis with High Surface Area Cu and K Promoted Reduced-Carbided Iron/Manganese Spinels. U.S. Patent US4621102, 1986.

(25) Soled, S. L.; Miseo, S.; Iglesia, E. Iron-Zinc Catalysts for the Conversion of Synthesis Gas to α-Olefins. U.S. Patent US5185378, 1993.

(26) Gül, Ö. F.; Ataç, Ö.; Boz, İ.; Özkara-Aydınoğlu, Ş. La, Mn and Zn Promoted Microporous Iron Catalysts with High Productivity and Stability for Fischer−Tropsch Synthesis. *React. Kinet., Mech. Catal.* **2016**, *117*, 147.
(27) Nam, S. S.; Lee, S. J.; Kim, H.; Jun, K. W.; Choi, M. J.; Lee, K. W. Catalytic Conversion of Carbon Dioxide into Hydrocarbons over Zinc Promoted Iron Catalysts. *Energy Convers. Manage.* **1997**, *38*, S397.
(28) Wang, H.; Yang, Y.; Xu, J.; Wang, H.; Ding, M.; Li, Y. Study of Bimetallic Interactions and Promoter Effects of FeZn, FeMn and FeCr Fischer−Tropsch Synthesis Catalysts. *J. Mol. Catal. A: Chem.* **2010**, *326*, 29.
(29) Maiti, G. C.; Malessa, R.; Baerns, M. Iron/manganese Oxide Catalysts for Fischer−Tropsch Synthesis. Part I: Structural and Textural Changes by Calcination, Reduction and Synthesis. *Appl. Catal.* **1983**, *5*, 151.
(30) Das, C. K.; Das, N. S.; Choudhury, D. P.; Ravichandran, G.; Chakrabarty, D. K. Hydrogenation of Carbon Monoxide on Unsupported Fe-Mn-K Catalysts for the Synthesis of Lower Alkenes: Promoter Effect of Manganese. *Appl. Catal., A* **1994**, *111*, 119.
(31) Zhang, J.; Lu, S.; Su, X.; Fan, S.; Ma, Q.; Zhao, T. Selective Formation of Light Olefins from CO_2 Hydrogenation over Fe−Zn−K Catalysts. *J. CO_2 Util.* **2015**, *12*, 95.
(32) Maiti, G. C.; Malessa, R.; Löchner, U.; Papp, H.; Baerns, M. Iron/manganese Oxide Catalysts for Fischer−Tropsch Synthesis. Part II: Crystal Phase Composition, Activity and Selectivity. *Appl. Catal.* **1985**, *16*, 215.
(33) Li, T.; Wang, H.; Yang, Y.; Xiang, H.; Li, Y. Effect of Manganese on the Catalytic Performance of an Iron-Manganese Bimetallic Catalyst for Light Olefin Synthesis. *J. Energy Chem.* **2013**, *22*, 624.
(34) Li, T.; Yang, Y.; Zhang, C.; An, X.; Wan, H.; Tao, Z.; Xiang, H.; Li, Y.; Yi, F.; Xu, B. Effect of Manganese on a Potassium-Promoted Iron-Based Fischer−Tropsch Synthesis Catalyst. *Fuel* **2007**, *86*, 921.
(35) Tao, Z.; Yang, Y.; Wan, H.; Li, T.; An, X.; Xiang, H.; Li, Y. Effect of Manganese on a Potassium-Promoted Iron-Based Fischer−Tropsch Synthesis Catalyst. *Catal. Lett.* **2007**, *114*, 161.
(36) Hu, B.; Frueh, S.; Garces, H. F.; Zhang, L.; Aindow, M.; Brooks, C.; Kreidler, E.; Suib, S. L. Selective Hydrogenation of CO_2 and CO to Useful Light Olefins over Octahedral Molecular Sieve Manganese Oxide Supported Iron Catalysts. *Appl. Catal., B* **2013**, *132*−*133*, 54.
(37) Cubeiro, M. L.; Valderrama, G.; Goldwasser, M. R.; Gonzalez-Jimenez, F.; Da Silva, M. C.; Perez-Zurita, M. J. Hydrogenation of CO and CO_2 with K and Mn Promoted Iron Catalysts. *Stud. Surf. Sci. Catal.* **1997**, *107*, 231.
(38) Satterfield, C. N.; Stenger, H. G. Fischer−Tropsch Synthesis on a Precipitated Manganese/iron Catalyst in a Well-Mixed Slurry Reactor. *Ind. Eng. Chem. Process Des. Dev.* **1984**, *23*, 26.
(39) Lee, J.; Chern, W.; Lee, M.; Dong, T. Hydrogenation of Carbon Dioxide on Iron Catalysts Doubly Promoted with Manganese and Potassium. *Can. J. Chem. Eng.* **1992**, *70*, 511.
(40) Martinelli, M.; Visconti, C. G.; Lietti, L.; Forzatti, P.; Bassano, C.; Deiana, P. CO_2 Reactivity on Fe−Zn−Cu−K Fischer−Tropsch Synthesis Catalysts with Different K-Loadings. *Catal. Today* **2014**, *228*, 77.
(41) Liang, M.; Kang, W.; Xie, K. Comparison of Reduction Behavior of Fe_2O_3, ZnO and $ZnFe_2O_4$ by TPR Technique. *J. Nat. Gas Chem.* **2009**, *18*, 110.
(42) Munteanu, G.; Ilieva, L.; Andreeva, D. Kinetic Parameters Obtained from TPR Data for α-Fe_2O_3 and Systems. *Thermochim. Acta* **1997**, *291*, 171.
(43) Li, S.; Meitzner, G.; Iglesia, E. Fischer−Tropsch Synthesis Catalysts Based on Fe Oxide Precursors Modified by Cu and K: Structure and Site Requirements. *Stud. Surf. Sci. Catal.* **2001**, *136*, 387.
(44) Xu, M.-W. P.; Brown, J. J. Mechanism of Iron Catalysis of Carbon Monoxide Decomposition in Refractories. *J. Am. Ceram. Soc.* **1989**, *72*, 110.
(45) Shroff, M. D.; Kalakkad, D. S.; Coulter, K. E.; Kohler, S. D.; Harrington, M. S.; Jackson, N. B.; Sault, A. G.; Datye, A. K. Activation of Precipeted Iron Fischer−Tropsch Synthesis Catalysts. *J. Catal.* **1995**, *156*, 185.
(46) Schulz, H.; Schaub, G.; Claeys, M.; Riedel, T. Transient Initial Kinetic Regimes of Fischer−Tropsch Synthesis. *Appl. Catal., A* **1999**, *186*, 215.
(47) Nakhaei Pour, A.; Housaindokht, M. R.; Tayyari, S. F.; Zarkesh, J.; Alaei, M. R. Deactivation Studies of Fischer−Tropsch Synthesis on Nano-Structured Iron Catalyst. *J. Mol. Catal. A: Chem.* **2010**, *330*, 112.
(48) de Smit, E.; Weckhuysen, B. M. The Renaissance of Iron-Based Fischer−Tropsch Synthesis: On the Multifaceted Catalyst Deactivation Behaviour. *Chem. Soc. Rev.* **2008**, *37*, 2758.
(49) Forzatti, P.; Lietti, L. Catalyst Deactivation. *Catal. Today* **1999**, *52*, 165.
(50) Sai Prasad, P. S.; Bae, J. W.; Jun, K.-W.; Lee, K.-W. Fischer−Tropsch Synthesis by Carbon Dioxide Hydrogenation on Fe-Based Catalysts. *Catal. Surv. Asia* **2008**, *12*, 170.
(51) Choi, P. H.; Jun, K.-W.; Lee, S.-J.; Choi, M.-J.; Lee, K.-W. Hydrogenation of Carbon Dioxide over Alumina Supported Fe-K Catalysts. *Catal. Lett.* **1996**, *40*, 115.
(52) Riedel, T.; Schaub, G.; Jun, K.-W.; Lee, K.-W. Kinetics of CO_2 Hydrogenation on a K-Promoted Fe Catalyst. *Ind. Eng. Chem. Res.* **2001**, *40*, 1355.
(53) Shi, B.; Davis, B. H. Fischer−Tropsch Synthesis: The Paraffin to Olefin Ratio as a Function of Carbon Number. *Catal. Today* **2005**, *106*, 129.
(54) Van Der Laan, G. P.; Beenackers, A. A. C. M. Kinetics and Selectivity of the Fischer−Tropsch Synthesis: A Literature Review. *Catal. Rev.: Sci. Eng.* **1999**, *41*, 255.
(55) Iglesia, E.; Reyes, S. C.; Madon, R. J.; Soled, S. L. Selectivity Control and Catalyst Design in the Fischer−Tropsch Synthesis: Sites, Pellets and Reactors. *Adv. Catal.* **1993**, *39*, 221.
(56) Tau, L. M.; Dabbagh, H. A.; Davis, B. H. Fischer−Tropsch Synthesis - Comparison of ^{14}C Distributions When Labeled Alcohol Is Added to the Synthesis Gas. *Energy Fuels* **1991**, *5*, 174.
(57) Ando, H.; Matsumura, Y.; Souma, Y. A Comparative Study on Hydrogenation of Carbon Dioxide and Carbon Monoxide over Iron Catalyst. *J. Mol. Catal. A: Chem.* **2000**, *154*, 23.
(58) Ojeda, M.; Li, A.; Nabar, R.; Nilekar, A. U.; Mavrikakis, M.; Iglesia, E. Kinetically Relevant Steps and H_2/D_2 Isotope Effects in Fischer−Tropsch Synthesis on Fe and Co Catalysts. *J. Phys. Chem. C* **2010**, *114*, 19761.
(59) Davis, B. H. *Technology Development for Iron and Cobalt Fischer−Tropsch Catalysts*; University of California at Berkeley: Berkely, CA, 2000.
(60) Tao, Z.; Yang, Y.; Zhang, C.; Li, T.; Ding, M.; Xiang, H.; Li, Y. Study of Manganese Promoter on a Precipitated Iron-Based Catalyst for Fischer−Tropsch Synthesis. *J. Nat. Gas Chem.* **2007**, *16*, 278.
(61) Zennaro, R.; Tagliabue, M.; Bartholomew, C. H. Kinetics of Fischer−Tropsch Synthesis on Titania-Supported Cobalt. *Catal. Today* **2000**, *58*, 309.